# Structure illumination microscopy imaging of lipid vescicles in live bacteria with naphthalimide-appended organometallic complexes

Electronic Supplementary Information

**Contents**

**Synthesis and Characterisation**

All reagents and solvents were purchased from Sigma Aldrich and used as received without further purification. Nuclear magnetic resonance spectra, consisting of $^{1}H$ and $^{13}C$ were recorded using a Bruker Advance 400 spectrometer (400.1 MHz for $^{1}H$, 100 MHz for $^{13}C$) at 300 K, or a Bruker 500 spectrometer (500.1 MHz for $^{1}H$, 125 MHz for $^{13}C$), using commercially available deuterated solvents. Spectra are reported in parts per million (ppm) downfield shift using trace solvent isotopic impurities as an internal reference. $^{1}H$ and $^{13}C$ chemical shifts were referenced to residual solvent signals. Elemental analyses were obtained at the School of Molecular and Life Sciences, Curtin University. High resolution ESI mass spectrometry was performed at The University of Sydney (Pt-**PyNapht**) and Edith Coward University (Re- **PyNapht**).

N-3-Aminopyridine-4-butylamino-1,8-naphtalimide (**PyNapht**):

A solution of 3-aminopyridine (85 mg, 0.90 mmol) and 4-nitro-naphthalic anhydride (200 g, 0.82 mmol) in ethanol (30 mL) was stirred at reflux for 16 h, then cooled to room temperature. The precipitate was filtered and then washed with cold ethanol and diethyl ether to give a beige solid. This crude residue was then combined with butylamine (35 μL, 3.5 mmol) in ethanol (30 mL) and stirred at reflux for 16 h. The reaction mixture was cooled and filtered, and the filtrate evaporated under reduced pressure. The crude solids were purified using silica column chromatography (0-10 % MeOH in $CH_2Cl_2$) to give **PyNapht** as a yellow solid (110 mg, 35%). $^{1}H$-NMR, $CDCl_3$, $\delta$ (ppm): 8.68 (s, b, 1H), 8.61-8.59 (m, 2H), 8.50 (d, $J$ = 4.0 Hz, 1H), 8.16 (d, $J$ = 8.0 Hz, 1H), 7.72-7.69 (m, 3H), 7.66-7.64 (m, 1H), 6.78 (d, $J$ = 8.0, 1H), 5.41 (s, b, 1H), 3.46-3.43 (m, 2H), 1.85-1.79 (m, 2H), 1.58-1.53 (m, 2H), 1.04 (t, $J$ = 7.4, 3H). $^{13}C$-NMR, $CDCl_3$, $\delta$ (ppm):164.8, 164.1, 150.2, 150.0, 149.1, 137.0, 135.3, 131.9, 130.5, 126.6, 124.9, 124.0, 123.9, 123.1, 120.5, 109.8, 104.7, 43.6, 31.2, 20.5, 14.0. HR-ESI: calculated for $C_{21}H_{19}N_3O_2$: 345.402 (*m/z*), found: 368.13695 (*m/z*) $[M+Na]^+$.

Pt-**PyNapht**:

Pt-**dmso** (0.050 g, 0.09 mmol) and **PyNapht** (0.060 g, 0.17 mmol) were dissolved in 5 mL of an acetone/MeOH (9:1) mixture. The reaction mixture was stirred at reflux overnight. After this time, the solvents were removed under reduced pressure. Purification *via* column chromatography, using silica as stationary phase and acetone as eluent, was required to yield the pure Pt-**PyNapht** (22 mg, 30%). $^{1}H$-NMR, acetone-$d_6$, $\delta$ (ppm): 8.67 (d, $J$ = 8.0 Hz, 1H), 8.64-8.63 (m, 1H), 8.58-8.44 (m, 3H), 8.21 (d, $J$ = 8.0 Hz, 1H), 7.96 (d, $J$ = 8.0 Hz, 2H), 7.88-7.79 (m, 2H), 7.73-7.68 (m, 2H), 7.59-7.51 (m, 3H), 7.23-7.00 (m, 7H), 6.93-6.90 (m, 1H), 3.56-3.39 (m, 2H), 1.86-1.79 (m, 2H), 1.57-1.50 (m, 2H), 1.01 (t, $J$ = 7.4 Hz, 3H). $^{13}C$-NMR, acetone-$d_6$, $\delta$ (ppm): 166.9, 163.7, 162.9, 153.5, 150.2, 150.0, 149.8, 137.4, 136.8,136.7, 132.8, 132.3, 130.8, 130.6, 130.2, 129.5, 129.5, 129.3, 128.0, 127.5, 125.5, 124.9, 124.7, 124.5, 123.6, 123.4, 113.4, 31.0, 20.4, 16.2. Two quaternary C peaks were not visible in the spectrum.

Aliphatic carbon peak overlapping with solvent signal. Anal. Calcd. for $C_{44}H_{35}N_4O_2Pt$: C 62.40%, H 4.17%, N 6.62%. Found: C 62.69%, H 4.07%, N 6.61%.

Re-**PyNapht**:

$[Re(CO)_3(phen)Br]$ was firstly prepared by reacting equimolar amounts of $[Re(CO)_5Br]$ and 1,10-phenanthroline in toluene at reflux for 4 hours. After this time, $[Re(CO)_3(phen)Br]$ was isolated via filtration and washing with diethyl ether. $[Re(CO)_3(phen)Br]$ (55 mg, 0.10 mmol) and $AgBF_4$ (20 mg, 0.10 mmol) were dissolved in acetonitrile and heated at reflux for 4 h while kept in the dark. The reaction mixture was cooled and filtered through celite to remove precipitated AgBr. **PyNapht** (36 mg, 0.10 mmol) was then added in the reaction mixture was heated at reflux for 24 h. After cooling to room temperature, the solvent was removed under reduced pressure. The obtained solids were dissolved in dichloromethane re-precipitate by addition of toluene. The crude product was filtered and purified by flash chromatography, using Brockmann III acidic alumina column as stationary phase. The starting materials were eluted with dichloromethane as the first fractions. The desired product was obtained by elution with ethyl acetate and the gradual addition of methanol up to 10%. To obtain an analytically pure sample, a further column was necessary using Brockmann II acidic alumina and the same ethyl acetate/methanol mixture as eluent. Yield: 6 mg (7%).$^1$H-NMR, DMSO-$d_6$, $\delta$ (ppm): 9.74 (d, $J$ = 5.1 Hz, 2H), 9.07 (d, $J$ = 8.3 Hz, 2H), 8.80 (d, $J$ = 8.5 Hz, 1H), 8.67 (s, 1H), 8.47 (d, $J$ = 8.0 Hz, 1H), 8.36 (s, 2H), 8.33 (d, $J$ = 7.3 Hz, 1H), 8.20-8.17 (m, 3H), 7.95-7.90 (m, 2H), 7.72-7.70 (m, 1H), 7.47-7.44 (m, 1H), 6.81 (d, $J$ = 8.6 Hz, 1H), 3.43-3.41 (m, 2H), 1.74-1.71 (m, 2H), 1.47-1.40 (m, 2H), 0.96 (t, $J$ = 7.4 Hz, 3H). Due to the low yield resulting from the synthetic procedure involved in the synthesis of Re- **PyNapht**, it was not possible to record a reliable $^{13}$C-NMR spectrum. Anal Calcd. for $C_{36}H_{27}N_5BF_4O_5Re \cdot CH_3OH$: C 48.59%, H 3.42%, N 7.66%. Found: C 48.46%, H 3.42%, N 7.25%.

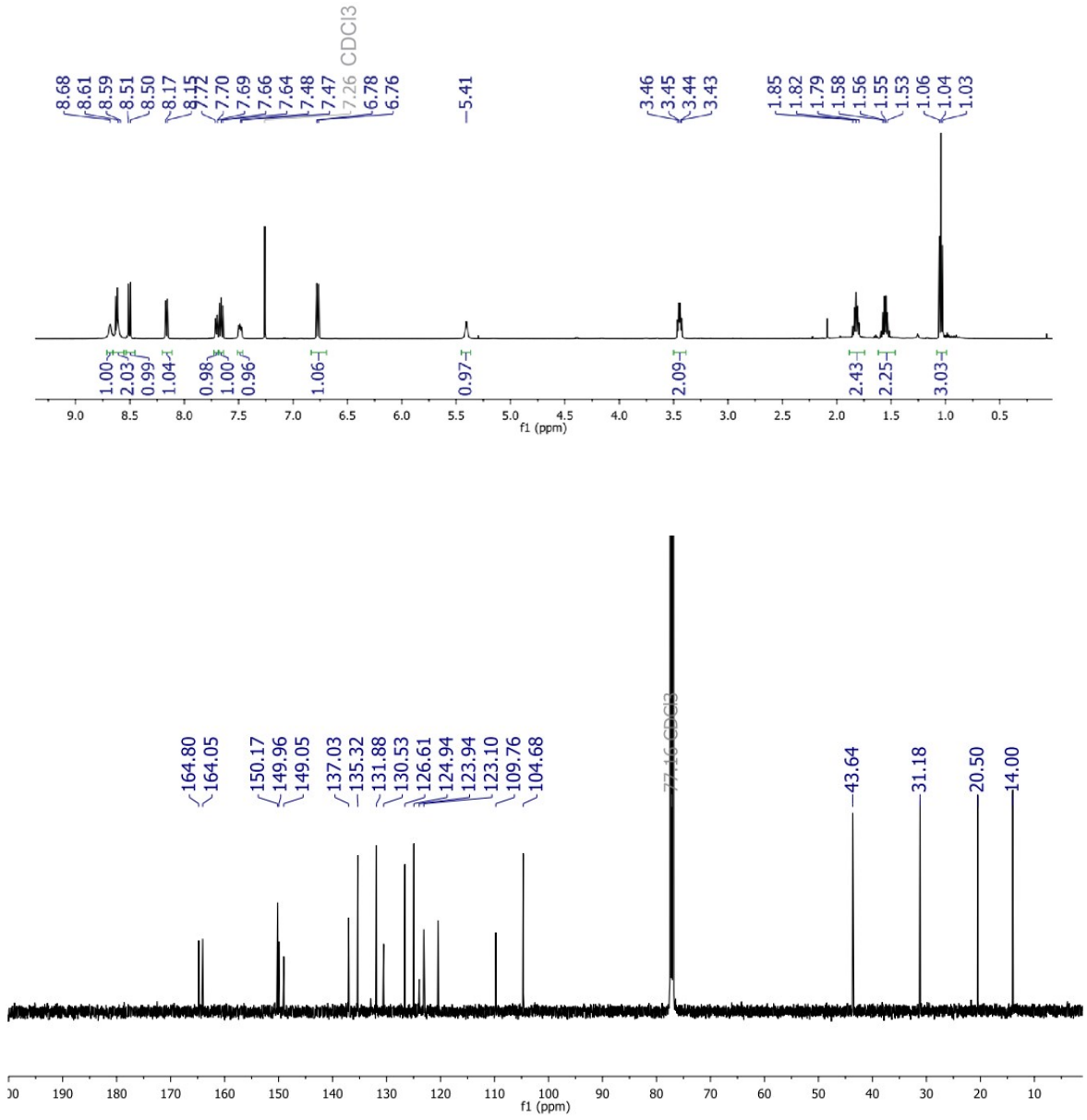


**Figure S1.** $^{1}H$ NMR (top) and $^{13}C$ NMR (bottom) of **PyNapht** in $CDCl_3$.

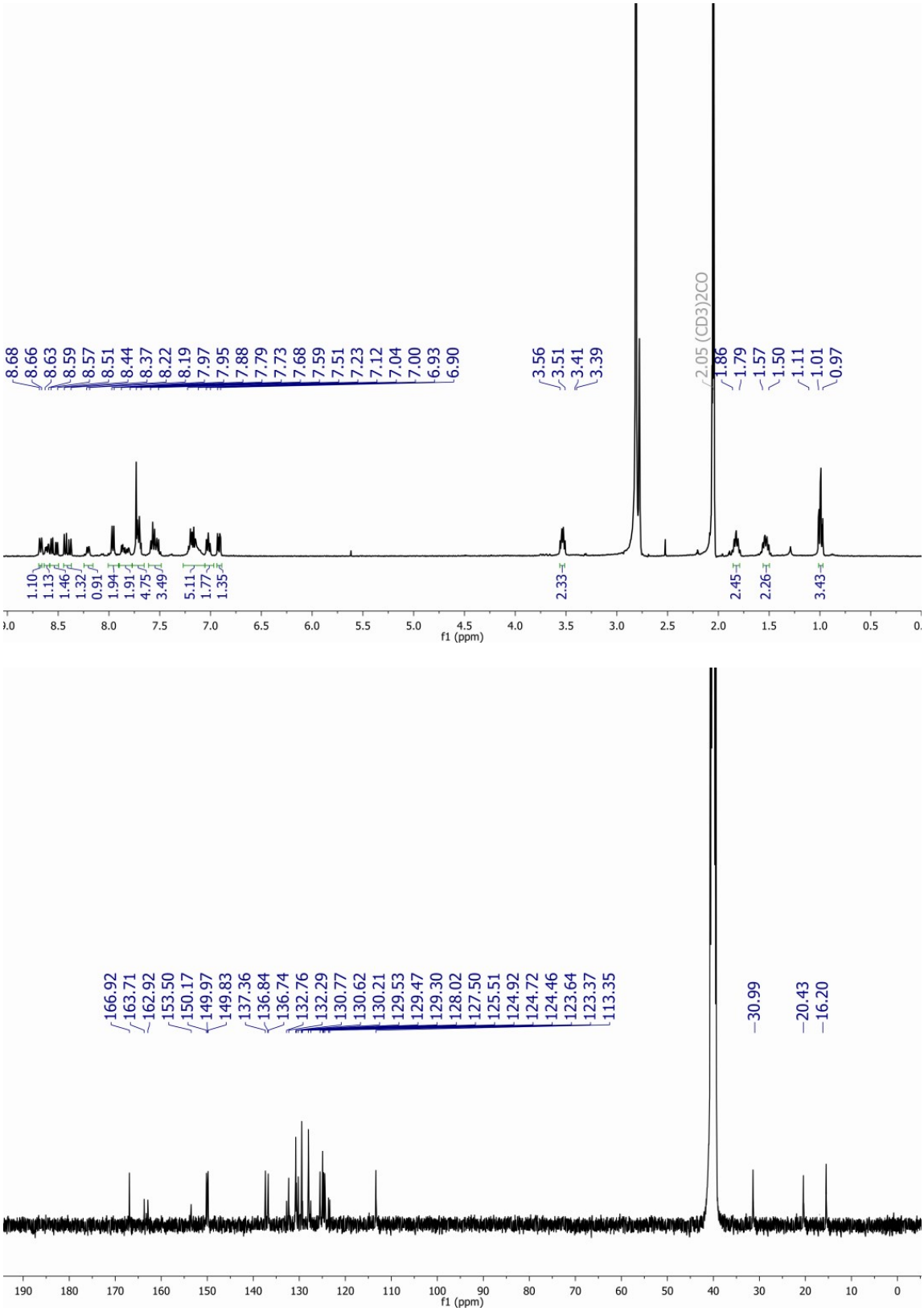


**Figure S2.** $^{1}$H NMR (top) and $^{13}$C NMR (bottom) of Pt-**PyNapht** in acetone-$d_6$.

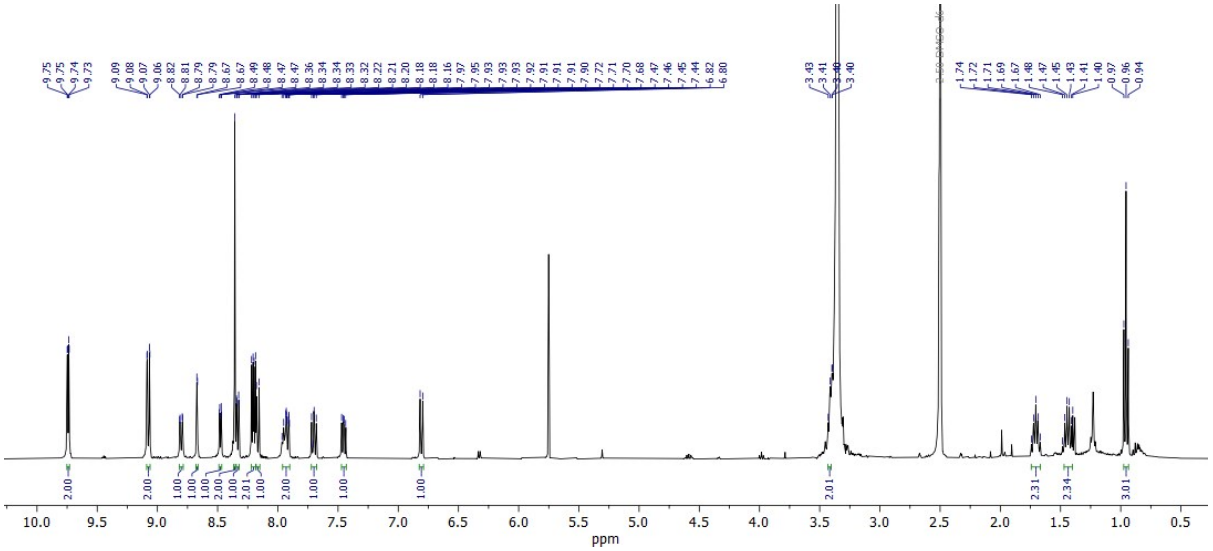


**Figure S3.** $^{1}$H NMR of Re-**PyNapht** in DMSO-$d_6$.

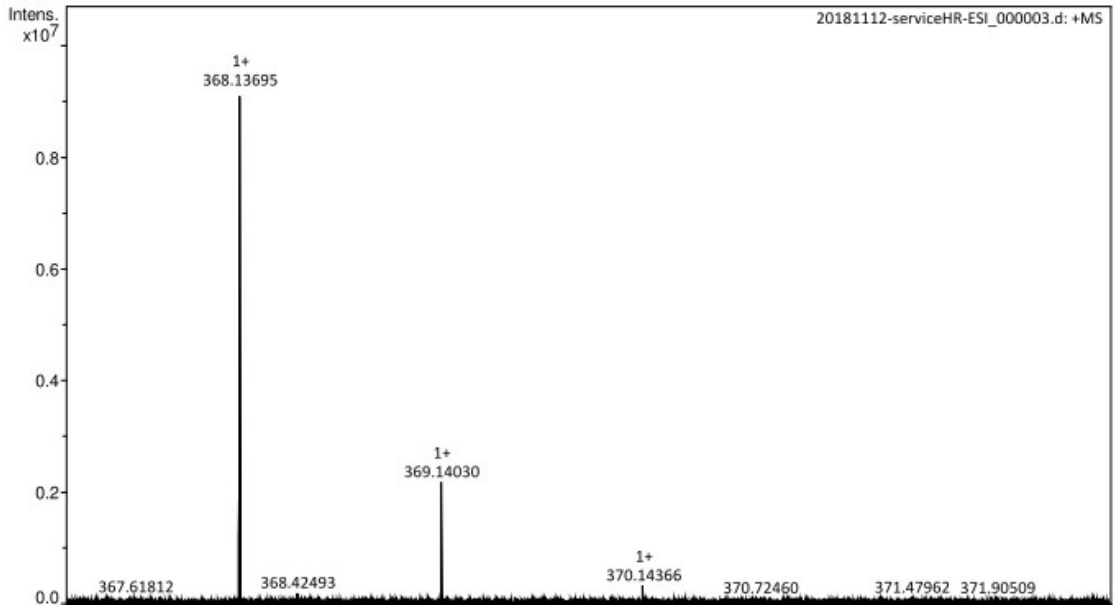


**Figure S4.** High resolution ESI mass spectrum of **PyNapht.**

**Photophysical Measurements**

Uncorrected steady state emission and excitation spectra were recorded on an Edinburgh FLSP980-S2S2-stm spectrometer equipped with: i) a temperature-monitored cuvette holder; ii) 450 W Xenon arc lamp; iii) double excitation and emission monochromators; iv) a Peltier cooled Hamamatsu R928P photomultiplier tube (spectral range 200-870 nm). Emission and excitation spectra were corrected for source intensity (lamp and grating) and emission spectral response (detector and grating) by a calibration curve supplied with the instrument. According to the approach described by Demas and Crosby,[1] luminescence quantum yields ($\Phi_{em}$) were measured in optically dilute solutions (O.D. < 0.1 at excitation wavelength) obtained from absorption spectra on a wavelength scale [nm] and compared to the reference emitter by Equation:

$$\Phi_x = \Phi_r \left[ \frac{A_r(\lambda_r) I_r(\lambda_r) n_x^2 D_x}{A_x(\lambda_x) I_x(\lambda_x) n_r^2 D_r} \right]$$

where $A$ is the absorbance at the excitation wavelength ($\lambda$), $I$ is the intensity of the excitation light at the excitation wavelength ($\lambda$), $n$ is the refractive index of the solvent, $D$ is the integrated intensity of the luminescence and $\Phi$ is the quantum yield. The subscripts $r$ and $x$ refer to the reference and the sample, respectively. The quantum yield determinations were performed at identical excitation wavelength for the sample and the reference, therefore cancelling the $I(\lambda_r)/I(\lambda_x)$ term in the equation. The quantum yields of complexes were measured against an aqueous solution of [Ru(**bipy**)$_3$]Cl$_2$ (**bipy** = 2,2'-bipyridine; $\Phi_r = 0.028$).[2] Emission lifetimes ($\tau$) were determined with the time correlated single photon counting technique (TCSPC) with the same Edinburgh FLSP980-S2S2-stm spectrometer using either a pulsed picosecond LED (EPLED/EPL 377 nm, FHWM < 800 ps). The goodness of fit was assessed by minimising the reduced $\chi^2$ function and by visual inspection of the weighted residuals. The solvents used for the preparation of the solutions for the photophysical investigations were of LR grade and the water was deionised. Degassing of the dichloromethane solutions was performed using the freeze-pump-thaw method. Experimental uncertainties are estimated to be ±8% for lifetime determinations, ±20% for quantum yields, ±2 nm and ±5 nm for absorption and emission peaks, respectively.

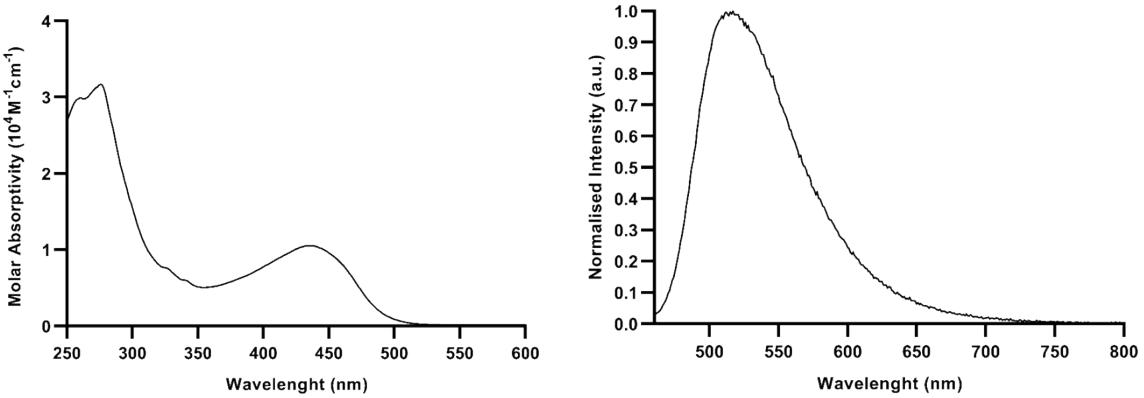


**Figure S5.** Absorption (left) and emission spectra (right) of Re-**PyNapht** from a *ca.* $10^{-5}$ M solution in DCM.

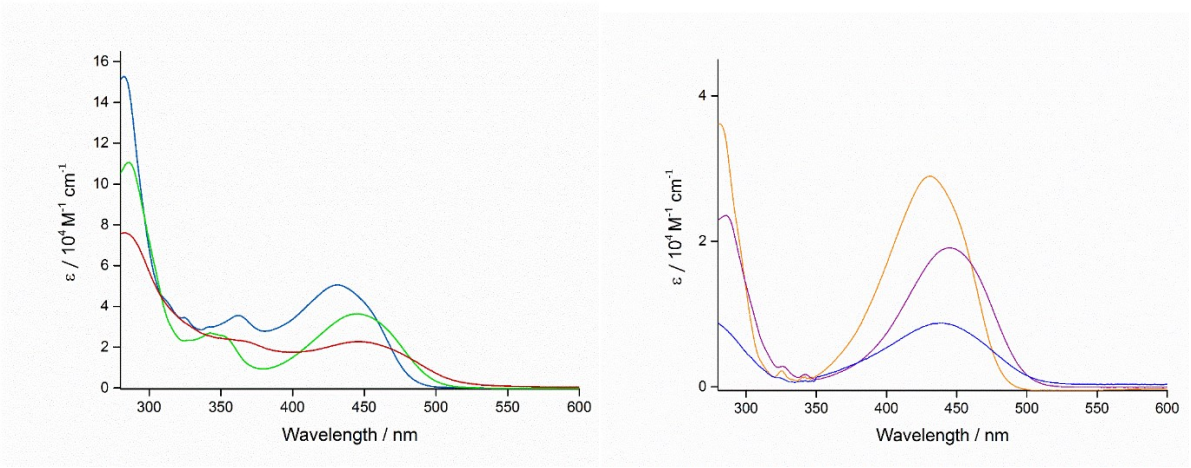


**Figure S6.** Left: Absorption spectra of Pt-**PyNapht** from $10^{-5}$ M solutions in DCM (blue line), DMSO (green line), $H_2O$ (red line). Right: absorption spectra of **PyNapht** from $10^{-5}$ M DCM (orange line), DMSO (purple line), $H_2O$ (blue line).

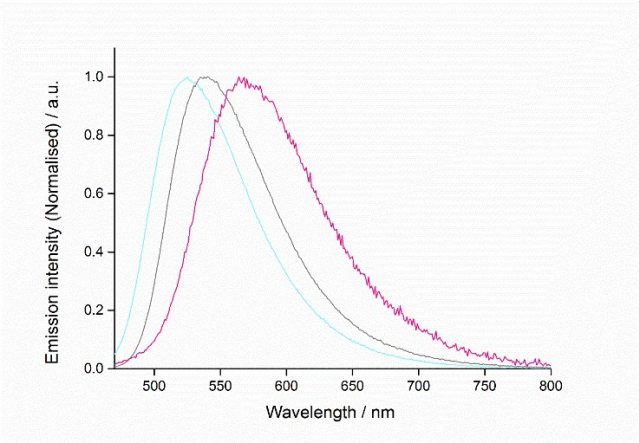


**Figure S7.** Emission spectra of **PyNapht** from $10^{-5}$ M DCM (light blue line), DMSO (grey line), $H_2O$ (pink line). $\lambda_{exc} = 430$ nm.

.

**Theoretical calculations**

To perform DFT and TD-DFT calculations, we have used the Gaussian16 program.[3] Our calculations consisted in geometry optimisations, vibrational spectra determinations, and TD-DFT calculations of **PyNaphth** and Pt-**PyNaphth**. We have applied default procedures, integration grids, algorithms and parameters, except for tighten energy (typically $10^{-10}$ a.u.) and internal forces ($10^{-5}$ a.u.) convergence thresholds. The ground-state ($S_0$) and excited-state ($S_1$) geometrical parameters have been determined with the M06-2X exchange-correlation functional. This choice was motivated by its relative high ratio of exact exchange (54%) limiting the formation of spurious charge-transfer excited-state that can sometimes be obtained with functionals encompassing smaller *exact* exchange ratio. The vibrational spectrum has been subsequently determined analytically at the same level of theory and it has been checked that all structures correspond to true minima of the potential energy surface for both $S_0$ and $S_1$. At least, the first thirty low-lying excited-states have been determined within the vertical TD-DFT approximation using the same functional, that is suited for optical spectra, though it tends to provide slightly too large transition energies.[4] For the structural and vibrational calculations, we have selected the 6-31G(d) atomic basis set for all atoms, but Pt that was treated with the LanL2DZ atomic basis set and pseudo-potential. For the TD-DFT calculations, we used the 6-311+G(2d,p) atomic basis set (light atoms) and the LanL08(f) basis/pseudopotential (Pt). During all steps, a modelling of bulk solvent effects (here DMSO) was achieved through the Polarizable Continuum Model (PCM).[5] For the TD-DFT calculations, we applied the linear-response[6] approach in its *non-equilibrium* limit and applied further corrections using the corrected linear-response[7] approach, so that all our values are "LR+cLR", i.e., includes both linear-response and state-specific solvent effects. The contour threshold used to draw the MOs was set to 0.02 au.

For **PyNaphth**, TD-DFT found that the lowest singlet excited state is strongly dipole allowed ($f$=0.46 for absorption and $f$=0.52 for emission). The computed vertical transition energies are at 3.21 eV (386 nm) for absorption and 2.59 eV (478 nm) for emission, both values being significantly blue-shifted compared to the measurements, as a logical consequence of the lack of vibronic corrections in such vertical estimates. Turning to data more directly comparable to experiment, the expected accuracy of TD-DFT is recovered, with a computed Stokes shift (5000 $cm^{-1}$) that fits reasonably well experiment (3950 $cm^{-1}$), and a theoretical 0-0 energy (2.77 eV or 448 nm) within an quarter of an eV from the measured crossing point between the absorption and emission curves (2.58 eV of 480 nm). For **PyNaphth** the lowest excited-state present a strongly dominant HOMO-LUMO character. These orbitals are displayed in Figure S8, and, as expected they are localized on the naphthalimide moiety and have a clear $\pi^*$ character. The partial CT character is also obvious with the HOMO more localised on the amino-donor group and two *bottom* rings whereas the LUMO shows a stronger contribution from the diimide moiety. Using Le Bahers' model, we computed an ICT of 0.60 e over 2.10 Å, which is a moderate CT character. For Pt-**PyNaphth**, the ground-state geometry reveals weakly interacting

chromophores (see Figure S9 and the main text). The lowest transition in Pt-**PyNaphth** is computed at 3.19 eV (389 nm, *f*=0.57) and corresponds to a HOMO-1 to LUMO transition, which has can be seen in Figure S8 are naphthalimide-centred and present the same shape has in **PyNaphth**. The three next higher transitions (378 nm, *f*=0.005; 343 nm, *f*=0.010; 308 nm, *f*=0.111) are all located on the Pt complex and account for the additional absorption band noticed experimentally. Consistently with the above, the optimization of the lowest singlet state leads to a bright emission (oscillator strength of 0.53) with a 0-0 energy at 2.78 eV (446 nm), almost unchanged from **PyNaphth**, as expected.

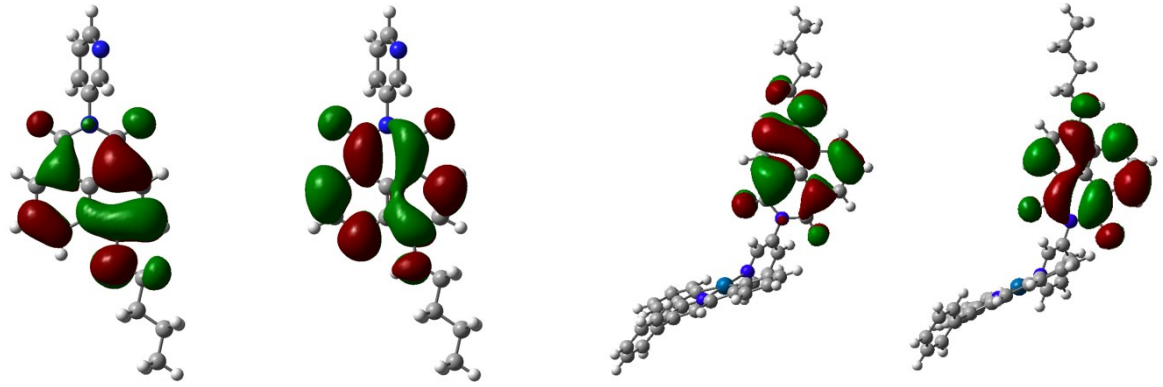

HOMO LUMO HOMO-1 LUMO

**Figure S8.** Relevant frontier MOs of **PyNaphth** (left) and Pt- **PyNaphth** (right).

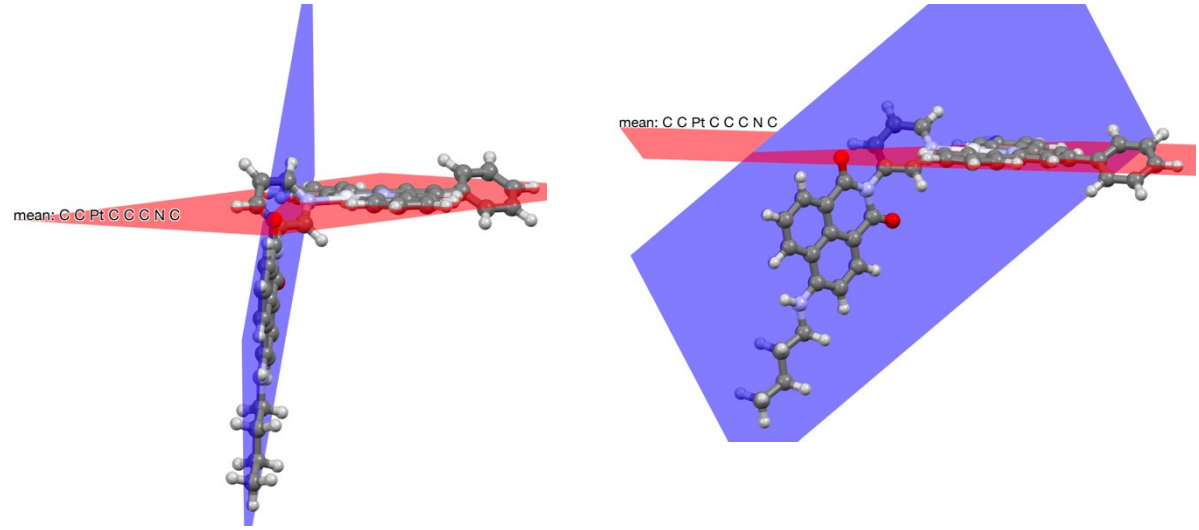


**Figure S9.** Two views of the optimal ground-state geometries of Pt-**PyNaphth**, with representations of the 1,8-naphthalmide and Pt-complex planes.

**Bacterial growth, staining and imaging conditions**

*Bacillus cereus* (ATCC10876) was used in this study. The bacterial strain was grown on Nutrient Broth agar plates at 37 °C. A bacterial culture was obtained by inoculating bacteria in Nutrient Broth media and incubating overnight in a shaking incubator at 37 °C.

Live bacteria were dosed with a 10 μM solution of Pt-**PyNapht** and **PyNapht** in Nutrient Broth (0.1% DMSO) for 15 minutes, then washed with Nutrient Broth and imaged. Staining with BODIPY 493/503 and MitoTracker Red (3 μM) was performed following the same protocol. Before imaging, bacteria were immobilised in a 1.5% Nutrient Agar gel. Super-resolution images were acquired using a Nikon SIM Ti2 inverted microscope equipped with a SR Apo TIRF AC 100xH oil immersion objective lens (NA = 1.49) and Andor DU-879 camera. All images were acquired as 3D SIM images, with 5 grating phases, and z-stacks steps of 0.12um, with a minimum of 7 slices. Pt-**PyNapht**, **PyNapht** and BODIPY were excited at 488 nm and the emission was collected in the 525/50 nm region. MitoTracker Red was excited at 561 nm and the emission collected in the 605/50 nm region. Images were collected and reconstructed using NIS-Element version 4.60.00 software. The images were processed using NIS-Element Viewer v.4.20 to select a specific z slice from the z stack acquired to show as much bacterium as possible, after which two images were generated: one showing the green channel and one showing both green and red channels. The final preparation of the collage was conducted with Adobe Photoshop CC (Adobe Systems Inc., USA), with no additional processing.

**NanoSIMS**

Bacteria were stained with the same protocol used for SIM imaging and fixed using 2% PFA. For the nanoSIMS imaging stained and fixed *B. cereus* were further processed using PELCO Biowave (Ted Pella, Inc.). Briefly, fixed *B. cereus* were washed with PBS for 3 times and then pre-embedded in agarose gel. Cell pellets in agarose gel were dehydrated in ethanol solution of 50%, 70%, 95%, 100%, and absolute acetone (2 times) for 40 s at 250W in the PELCO Biowave. Araldite-Epon resin was used for cell embedding with infiltration at 25%, 50%, 75% resin in absolute acetone, and 100% resin (2 times) in the PELCO Biowave under vacuum at 250W for 2 min. Cell pellets were then cured in 70 ºC oven for overnight.

500 nm sections were cut with a Leica UC6 ultramicrotome and mounted on silicon wafers. Sections were coated with a thin layer of gold and imaged with NanoSIMS 50 (CAMECA). Secondary ions ($^{12}C^{14}N^-$, $^{32}S^-$ and $^{195}Pt^-$) were collected. Selected regions of the section were scanned before imaging (primary aperture D1=1) to remove the gold coating and ensure a steady state of secondary ion release. A 15 × 15-µm region was imaged with an ~3-pA beam current (primary aperture D1=2) and a dwell time of 30 ms/pixel per frame for four frames. 256×256–pixel images were obtained. Images were prepared using the OpenMIMS plugin in ImageJ. $^{195}Pt^-$ image was processed with a mean filter with a radius of 3 pixels.

**Super-resolution and confocal images**

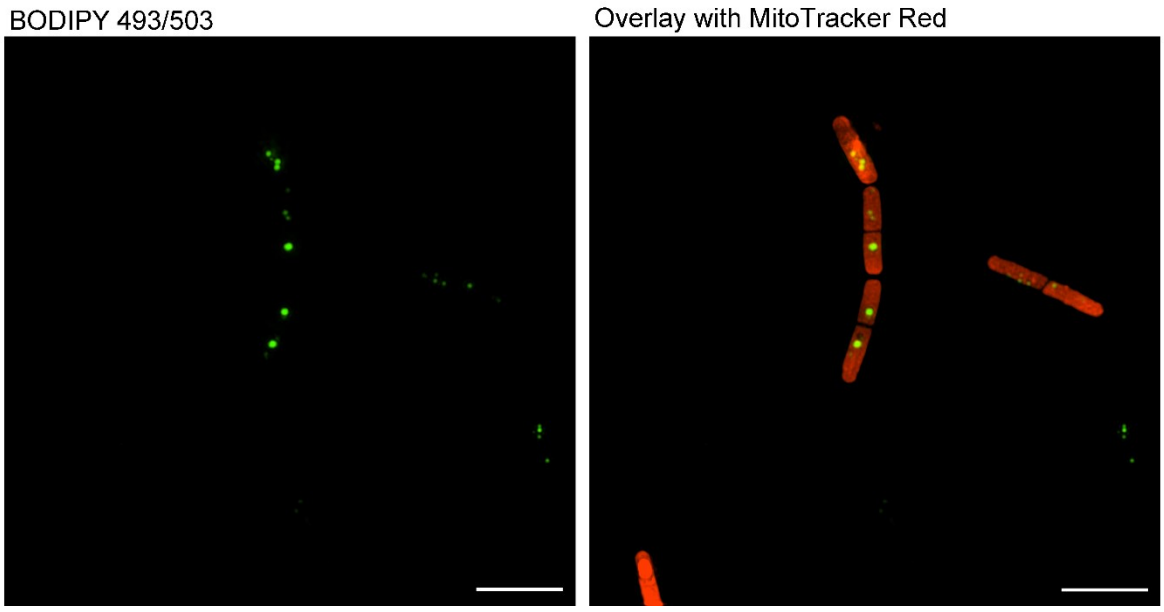


**Figure S10.** SIM images of live *B. cereus* incubated with BODIPY (left) and co-stained with MitoTracker Red (right). BODIPY 493/503 was excited at 488 nm and the emission collected in the 252/50 nm region. MitoTracker Red was excited at 561 nm and the emission collected in the 605/50 region. Scale bars: 5 μm.

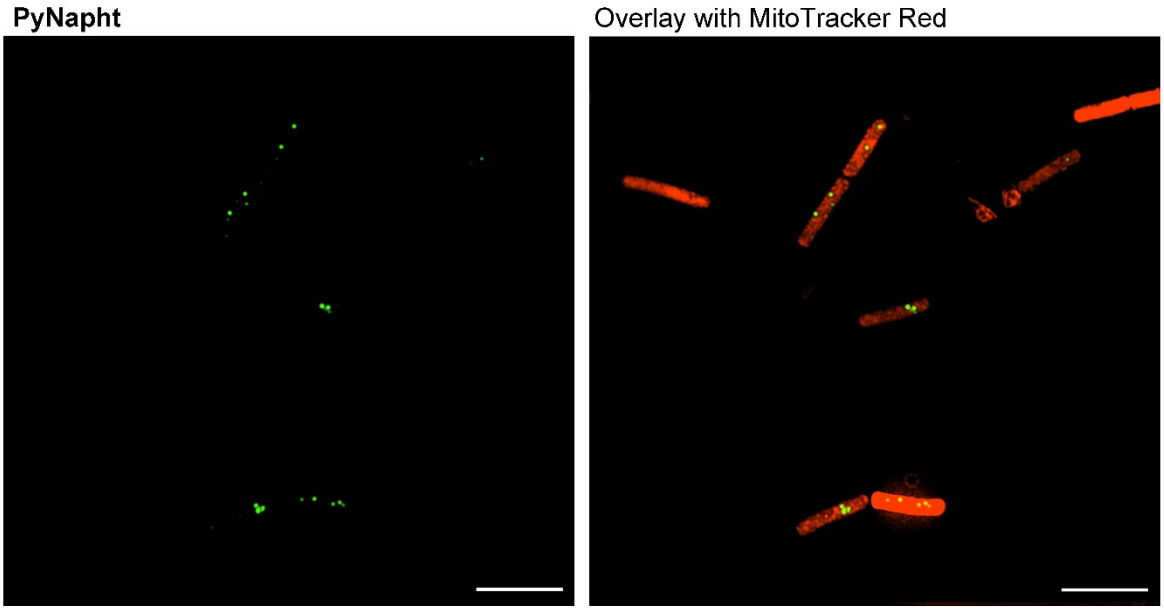


**Figure S11** SIM images of live *B. cereus* incubated with **PyNapht** (left) and co-stained with MitoTracker Red (right). **PyNapht** was excited at 488 nm and the emission collected in the 252/50 nm region. MitoTracker Red was excited at 561 nm and the emission collected in the 605/50 region. Scale bars: 5 μm

**References**


[1] G. A. Crosby, J. N. Demas, *J. Phys. Chem.* **1971**, *75*, 991-1024.

[2] K. Nakamaru, *Bull. Chem. Soc. Jpn.* **1982**, *55*, 2697-2705.

[3] M. J. Frisch, **2016**, pp. Wallingford, USA.

[4] D. Jacquemin, E. A. Perpte, I. Ciofini, C. Adamo, R. Valero, Y. Zhao, D. G. Truhlar, *J. Chem. Theory Comput.* **2010**, *6*, 2071-2085.

[5] J. Tomasi, B. Mennucci, R. Cammi, *Chem. Rev.* **2005**, *105*, 2999-3094.

[6] R. Cammi, B. Mennucci, *J. Chem. Phys.* **1999**, *110*, 9877-9886.

[7] M. Caricato, B. Mennucci, J. Tomasi, F. Ingrosso, R. Cammi, S. Corni, G. Scalmani, *J. Chem. Phys.* **2006**, *124*, 1-13.